Segmentation-Based Registration of Organs in Intraoperative Video Sequences

James Goddard[1*], Timothy Gee[1], Hengliang Wang[2] and Alexander M. Gorbach[3]
[1]Image Science and Machine Vision Group, Oak Ridge National Laboratory, Oak Ridge, Tennessee 37831
goddardjsjr@ornl.gov, geetf@ornl.gov
[2]Naval Medical Research Center, Silver Spring, Maryland 20910
wangheng@mail.nih.gov
[3]National Institutes of Health, Bethesda, Maryland 20892
gorbach@helix.nih.gov

Abstract. Intraoperative optical imaging of exposed organs in visible, near-infrared, and infrared (IR) wavelengths in the body has the potential to be useful for real-time assessment of organ viability and image guidance during surgical intervention. However, the motion of the internal organs presents significant challenges for fast analysis of recorded 2D video sequences. The movement observed during surgery, due to respiration, cardiac motion, blood flow, and mechanical shift accompanying the surgical intervention, causes organ reflection in the image sequence, making optical measurements for further analysis challenging. Correcting alignment is difficult in that the motion is not uniform over the image. This paper describes a Canny edge-based method for segmentation of the specific organ or region under study, along with a moment-based registration method for the segmented region. Experimental results are provided for a set of intraoperative IR image sequences.

1 Introduction

Intraoperative optical images of exposed organs in visible, near-infrared, and infrared (IR) wavelengths in the body have the potential to be useful for real-time, non-invasive assessment of organ viability and image guidance during surgical intervention. Relatively low cost, non-invasiveness and good specificity for physiological changes make optical imaging desirable for a variety of surgical procedures [1-4]. However, the motion of the internal organs presents significant challenge for real-time data analysis of recorded two-dimensional video sequences.

The movement of the kidney, liver, urethra, etc. observed during surgery due to respiration, cardiac motion, and blood flow, can be between 15 and 20 mm. In addition to mechanical shift of the tissue from the surgical intervention, all of these cause organ reflection in the image sequence, making optical measurements for further analysis

* Prepared by Oak Ridge National Laboratory, managed by UT-Battelle, LLC, for the U.S.Department of Energy under Contract No. DE-AC05-00OR22725.

challenging. Correcting alignment is difficult in that the motion is not uniform over the image. Also, other artifacts, such as glare caused by illumination from surgical lights reflecting off of wet tissue surfaces (in the case of visible wavelength imaging) and evaporative cooling (in IR imaging), add random noise to the imagery, do not allow clear visualization of internal fiducial markers, and, therefore, make the task more difficult.

This paper describes a Canny edge-based method for segmentation of the specific organ or region under study, along with a shape moment-based registration method for the segmented region. Experimental results are provided for a set of intraoperative IR image sequences of the kidney. All organs generally exhibit 3D motions, in addition to having 3D volumes. Moreover, these organs and tissues are surrounded by deformable surfaces. While medical image registration has been well-researched [5-12], the registration to two-dimensional IR surgical image sequences to non-rigid 3D structures has not been extensively studied.

2 Image Registration Method

Image registration for an IR video is accomplished in two stages. The organ or region of interest is first automatically segmented throughout the video sequence. This process is accomplished by a combination of edge extraction and morphological operations that form a closed boundary of the organ. Then a shape-based registration algorithm is applied to the segmented organ to estimate the alignment error relative to a base image in the image sequence. These steps are detailed below.

2.1 Image Sequence Collection

IR imaging sequences of porcine kidney were collected to evaluate renal ischemia, particularly focal perfusion deficits. Laparotomy with renal mobilization, hilar dissection, and identification of segmental branches were performed in six porcine models. An IR camera (3-5 μ wavelengths) was directed at two exposed kidneys from 30 cm distance. Images (320x256x14 bits) were collected at the rate of one per second with 300-600 images per sequence.

These image sequences have been used for development and testing of the registration method. Figure 1(a) shows a baseline IR image of a pig kidney collected during this evaluation. An outline of the kidney edge generated by the segmentation method is also shown in Figure 1(b). At this boundary, the contrast with the surrounding tissue varies from good to just visible.

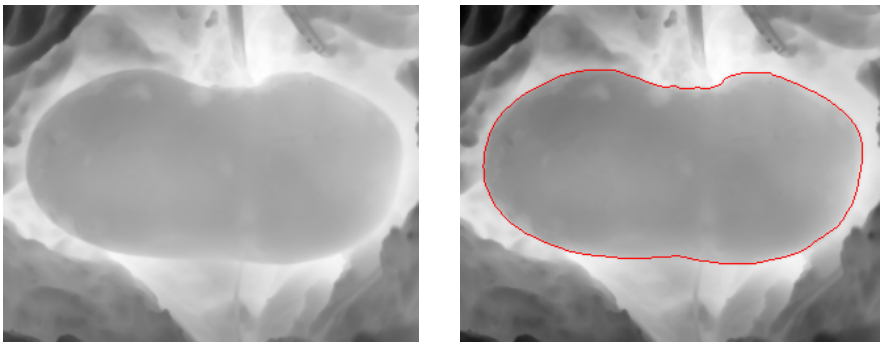

(a) (b)

Figure 1. IR image of pig kidney from video sequence shows varying contrast at kidney boundary. (a) shows original image while (b) shows an overlay of the kidney contour

As a preprocessing step, 2D median filtering is applied to remove fixed pattern noise present after calibration of the IR images. The improved result is shown below in Figure 2.

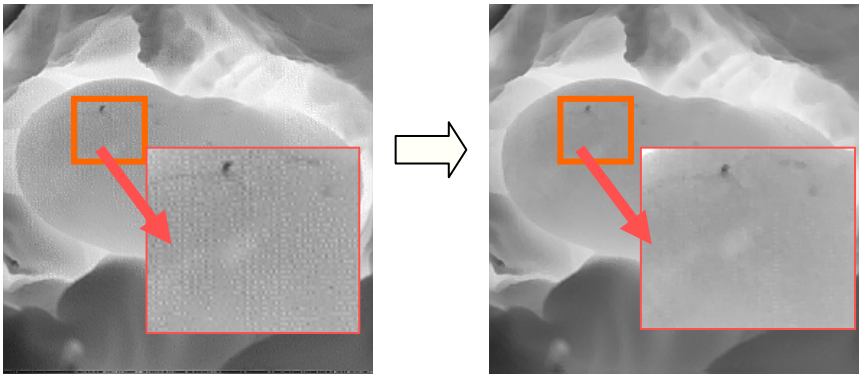

Figure 2. 2D median filtering with a 3 by 3 window is applied to each input image to reduce fixed pattern noise as shown in the image insets

2.2 Organ Segmentation

In the acquired video, the kidney is moving in the foreground with the pig's other body organs in the background. The image content at the boundary of the kidney is changing slightly since the kidney is not fixed to the background at its edges. Therefore to achieve good video registration it is necessary to segment the organ from the background and consider it independently.

In much of the imagery, the overall contrast between the kidney and the overall background is useful. With this in mind, we can achieve segmentation using a Canny [13] edge finder followed by some morphological operations. Figure 3(a) shows the result following the Canny edge detection.

From the Canny edge detection, a binary image is obtained, in which edge pixels have the value 1, and other pixels are 0. This image is the input of morphological operations performed to acquire the kidney as an object. The first operation is *bridging* which joins pixels of value 1 that are separated by only one zero pixel. This fills gaps in the kidney contour. In some cases, it was necessary to dilate the edge image before bridging to allow bigger gaps to be filled. In these cases the edge was thinned afterward [14].

After bridging, an image fill operation is performed that starts at the center of the kidney and inserts values of 1 until stopped by a continuous boundary of 1s. If the kidney boundary was extracted without gaps, then this operation creates a binary object describing the kidney. If there are gaps in the boundary, then the fill operation will fill a much greater area than the size of the kidney and will likely fill the entire image. This case is easily detected, leading us to use the kidney object obtained from the previous frame. However, if good contrast is available, the above procedure obtains the boundary with a high success rate.

After the image fill, binary connectivity analysis is performed so that the kidney can be identified as an object. An operation is then performed to fill any holes in this object, so that the kidney is completely covered. Additional morphological operations such as *opening* (erosion followed by dilation) are necessary to remove small appendages of the kidney that occur from background edges that are adjacent to the kidney. The result is a single object that only describes the kidney shape and location, as shown in Figure 3(b).

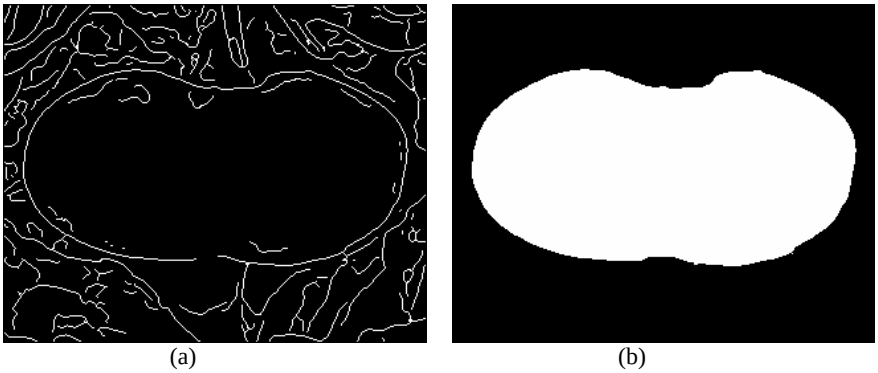

(a) (b)

Figure 3. Canny edge (a) and segmented kidney (b) image

2.3 Registration

In the video that we have observed, the kidney is well-approximated as a rigid body. During the organ's movements, the background changes, and the kidney's location and rotation in the background changes, but the kidney's shape does not change significantly. Therefore, it's possible to perform registration using the object location and orientation that was extracted as described above. We have experimented with the use of tracking intensity textures or landmarks within the kidney region, but we have found the most accurate and robust results from tracking the kidney's contour.

As illustrated in Figure 4, by using first and second-order moments [14] of the obtained binary object, we can describe its location and orientation. The first-order moments, or centroid, define the x and y coordinates of the object's center of mass. The second-order central moments can be used to define the object's axis of maximum elongation. Here, the shape is modeled as an ellipse, and we find the angle of the major axis of an ellipse with the same second-order central moments as the binarized kidney.

The segmented kidney object in the first frame of the image sequence is used as a reference. The registration of each following frame is then defined by the translation needed to shift the centroid and align the major axis to match the reference. This defines a homogenous transform to map intensity values from image points in the current frame to the corresponding locations of the reference image. Since subpixel locations are needed from the current frame, interpolation is required. We have found bi-cubic interpolation to be sufficient.

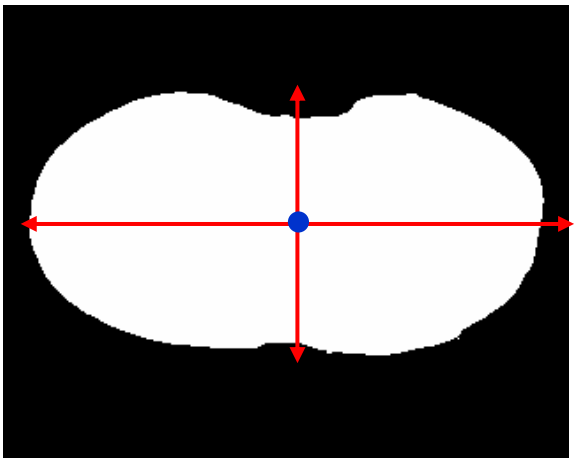

Figure 4. Illustration of first and second-order moments in the segmented kidney object

3 Experimental Results

The registration method described in section 2 has been applied to five sequences of intraoperative IR pig kidney images. The resulting registered image sets have been evaluated using both a cross-correlation and a frequency-based measure. Typical results from each of these measures are given below.

3.1 Cross-correlation registration performance measure

The normalized cross-correlation value S is provided in Eq. (1), which allows computing pixel-wise cross-correlation coefficients between the pixel intensities of the two images, normalized by the square root of their autocorrelations.

$$S(d_x, d_y) = \frac{\sum_{(x,y)\in C}[I_1(x+d_x, y+d_y) - \overline{I_1(x+d_x, y+d_y)}]*[I_2(x,y) - \overline{I_2(x,y)}]}{\sqrt{\sum_{(x,y)\in C}[I_1(x+d_x, y+d_y) - \overline{I_1(x+d_x, y+d_y)}]^2 * \sum_{(x,y)\in C}[I_2(x,y) - \overline{I_2(x,y)}]^2}} \quad (1)$$

where I_1, I_2 are intensities of the two images respectively, C is the mask of the image, d_x, d_y are number of shifting pixels in x and y directions. The mask is such that the cross-correlation is performed only on interior pixels of the kidney.

When S reaches the maximum value, $d_x = d_{xmax}$, $d_y = d_{ymax}$. Then $D = |d_{xmax}| + |d_{ymax}|$, is defined as the number of shifting pixels. Ideally, for the two perfect registered images, $D = 0$. The smaller D value is, the less the motion affects the image sequence. The D values between each adjacent renal IR images are calculated to test the performance of image registration.

The numbers of shifting pixels (D value) for each image in the sequence before and after registration were calculated (see Figure 5). The mean D values for whole sequence are 1.8 for non-registered image sequence vs. 0.7 for registered image sequence. While the actual registration is at a subpixel level, the reduction in integer correlation shifts of the kidney interior proves the stabilization in kidney position for this sequence.

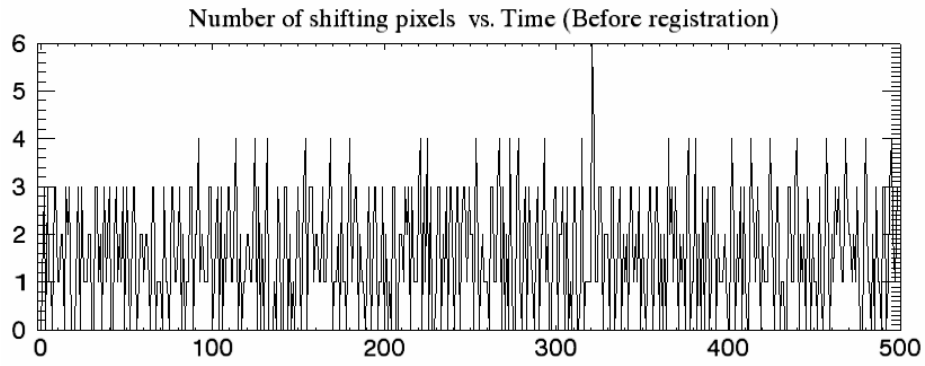

(a)

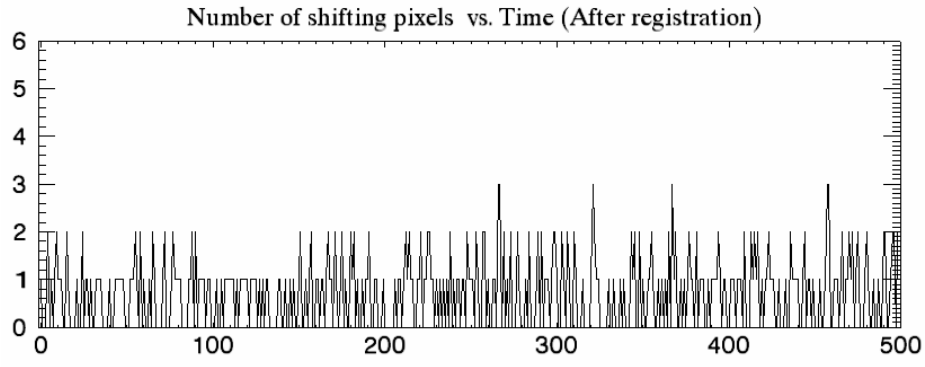

(b)

Figure 5. Comparison of number of shifting pixels (D values) between two sequences of 500 images each: before (a) and after (b) registration

3.2 Frequency domain registration performance measure

A frequency domain analysis to measure alignment was performed on an interior image region of the kidney. For this test, a 21 by 21 pixel region was used. The mean value for this region was calculated for each image in the sequence. Figure 6 shows the before and after registration for one such typical region over the sequence. The time sequence before registration is seen to have higher noise than after registration.

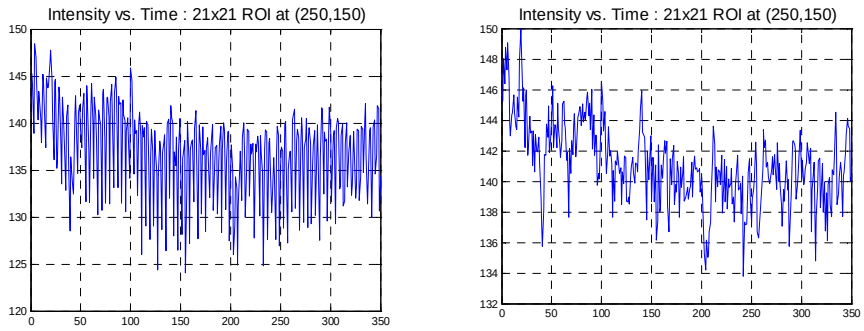

(a) (b)

Figure 6. Time domain plot of 21 by 21 pixel region mean value for all images in sequence before registration (a) and after registration (b). A significant reduction in noise level can be seen after registration

The discrete Fourier transform (DFT), f_k for $k = 0 \ldots N-1$, is calculated for the time sequence t_n for $n = 0 \ldots N-1$,

$$f_k = \sum_{n=0}^{N-1} t_n e^{-\frac{2\pi i n k}{N}} . \tag{2}$$

The frequency domain plot of the DFT gives further insight into the registration effectiveness. Figure 7(a) shows a large frequency component located approximately 0.25 of Nyquist. This component has a period of 4 seconds where the sampling frequency is 1/sec. and corresponds to the respiration rate. Figure 7(b) shows that this component is reduced to background noise levels after registration. The registration method removed the motion corresponding to the respiration.

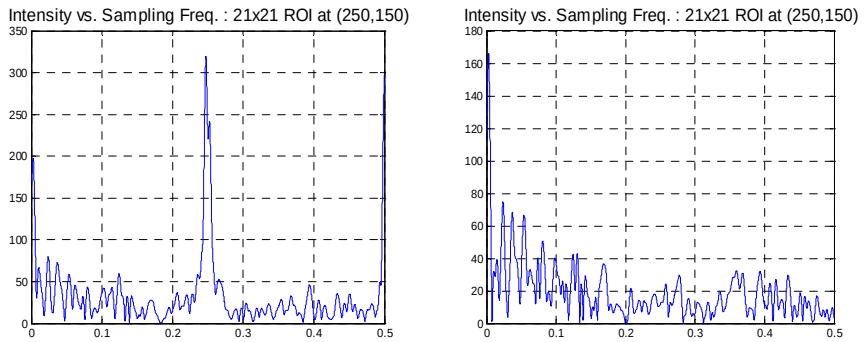

(a) (b)

Figure 7. Discrete Fourier transform of 21 by 21 pixel region mean value as shown in Figure 6 before registration (a) and after registration (b). DFT shows elimination of significant frequency band (due to respiration-induced movement) after registration

4 Conclusions

An image sequence registration method has been proposed that provides localized registration for specific regions and organs in intraoperative 2D medical image sequences. The IR image sets presented challenges due to thermal noise and low contrast. Successful segmentation of the kidney in these images was achieved using this method and good overall registration was applied to these regions. Performance results were presented that demonstrated quantitatively the improvement in the image alignment. This method can be applied not only to IR imagery but to visible optical images as well. Additional work is needed to characterize the thermal noise and to reduce the effects on the registration and measured thermal signals. This method is capable of being implemented in real-time using available hardware and software.

References

1. Gorbach A, Simonton D, Hale DA, Swanson SJ, Kirk AD. Objective, real-time, intraoperative assessment of renal perfusion using infrared imaging. Am J Transplant. 2003 Aug;3(8):988-93.
2. Gorbach AM, Heiss JD, Kopylev L, Oldfield EH. Intraoperative infrared imaging of brain tumors. J Neurosurg. 2004 Dec;101(6):960-9.
3. Reuthebuch O, Haussler A, Genoni M, Tavakoli R, Odavic D, Kadner A, Turina M. Novadaq SPY: intraoperative quality assessment in off-pump coronary artery bypass grafting. Chest. 2004 Feb;125(2):418-24.
4. Mitsuta H, Ohdan H, Fudaba Y, Irei T, Tashiro H, Itamoto T, Asahara T. Near-infrared spectroscopic analysis of hemodynamics and mitochondrial redox in right lobe grafts in living-donor liver transplantation. Am J Transplant. 2006 Apr;6(4):797-805.
5. A. Bardera, M. Feixas, I. Boada, “Normalized similarity measures for medical image registration,” SPIE Medical Imaging, Proceedings of SPIE, Vol. 5370, 2004.
6. J. Pluim, J. Maintz, M. Viergever, “Mutual information based registration of medical images: a survey,” IEEE Transactions on Medical Imaging, Vol.22, No. 8, 2003.
7. J. Ruiz-Alzola, E. Suarez, C. Alberola-Lopez, S.K. Warfield, C.-F Westin, “Geostatistical Medical Image Registration,” MICCAI 2003, LNCS 2879, Springer-Verlag, 2003.
8. J. Maintz, P. van den Elsen, M. Viergever, “3D multimodality image registration using morphological tools,” Image and Vision Computing, Vol. 19, Elsevier, 2001.
9. C. Sorzano, P. Thevenaz, and M. Unser, “Elastic Registration of Biological Images UsingVector-Spline Regularization,” IEEE Transactions on Biomedical Engineering, Vol. 52, No. 4, pp 652-663, April, 2005.
10. B. Lucas and T. Kanade, “An iterative image registration technique with an application to stereo vision,” in DARPA Image Understanding Workshop. DARPA, 1981, pp. 121–130.
11. Maes, F., “Medical image registration using mutual information,” *Proceedings of the IEEE*, v 91, n 10, October, 2003, pp 1699-1721.
12. C. Davatzikos, J. L. Prince, and R. N. Bryan, “Image Registration Based on Boundary Mapping”, IEEE Transactions on Medical Imaging, Vol. 15, No. 1, Feb. 1996.
13. Canny, John, "A Computational Approach to Edge Detection," IEEE Transactions on Pattern Analysis and Machine Intelligence,Vol. PAMI-8, No. 6, 1986, pp. 679-698.
14. Haralick, Robert M., and Linda G. Shapiro, *Computer and Robot Vision*, Volume I, Addison-Wesley, 1992.